

Stimulated Raman scattering microscopy with a robust fibre laser source

Christian W. Freudiger^{1,2†}, Wenlong Yang^{2†}, Gary R. Holtom², Nasser Peyghambarian³, X. Sunney Xie^{2*} and Khanh Q. Kieu^{3*}

Stimulated Raman scattering microscopy allows label-free chemical imaging and has enabled exciting applications in biology, material science and medicine. It provides a major advantage in imaging speed over spontaneous Raman scattering and has improved image contrast and spectral fidelity compared to coherent anti-Stokes Raman scattering. Wider adoption of the technique has, however, been hindered by the need for a costly and environmentally sensitive tunable ultrafast dual-wavelength source. We present the development of an optimized all-fibre laser system based on the optical synchronization of two picosecond power amplifiers. To circumvent the high-frequency laser noise intrinsic to amplified fibre lasers, we have further developed a high-speed noise cancellation system based on voltage-subtraction autobalanced detection. We demonstrate uncompromised imaging performance of our fibre-laser-based stimulated Raman scattering microscope with shot-noise-limited sensitivity and an imaging speed up to 1 frame s⁻¹.

In coherent Raman scattering (CRS) microscopy^{1–6}, the sample is illuminated with two synchronized laser beams, which are commonly referred to as pump and Stokes. If their frequency difference matches a molecular vibrational frequency of the sample, the targeted population is excited from the ground to the vibrational state (Fig. 1a)⁷. In contrast to spontaneous Raman scattering, the stimulated transition from the virtual to the vibrational state by the presence of the Stokes field results in an amplification of the molecular transition rate and allows label-free chemical imaging at speeds up to video rate^{8,9}.

Various detection schemes have been developed to probe this amplified Raman signal in microscopy. The easier to implement coherent anti-Stokes Raman scattering (CARS)^{1,2} suffers from a non-resonant background signal that limits sensitivity for dilute species^{10,11}. Stimulated Raman scattering (SRS) is free from this background and its excitation spectra match well-documented spontaneous Raman spectra^{3–6}. The typical implementation of SRS¹² detects the small intensity loss of the transmitted pump beam with a high-frequency modulation transfer scheme that takes advantage of the fact that laser noise of solid-state lasers commonly reduces to shot noise at high frequencies¹³.

SRS has been applied extensively in biomedical research¹⁴, and achieving high sensitivity under biocompatible excitation conditions is a key challenge. As a nonlinear optical process, SRS benefits from the use of pulsed near-infrared lasers, which generate high signal levels at a moderate average power. The best signal levels are obtained by narrowband excitation of a single vibrational frequency. Species with spectrally mixed bands can be distinguished by multispectral imaging, where the frequency difference of the pump and Stokes beams is tuned between image frames^{15,16} or lines¹⁷. An ideal light source for SRS provides two tightly synchronized and quickly tunable pulse trains with bandwidths narrower than a typical Raman linewidth (<20 cm⁻¹).

The current gold-standard laser system for SRS is a synchronously pumped picosecond optical parametric oscillator (OPO)¹⁸, which has vanishing timing jitter compared to electronically

synchronized lasers¹⁹. Its cost is high and the free-space cavity is sensitive to environmental changes. Fibre-laser technology has the potential to overcome these limitations as its components are inexpensive and light guiding by the fibre core avoids misalignment. Different concepts have been proposed^{20–26}. From the free-space OPO system we have learned that optical synchronization avoids timing jitter and improves long-term stability. However, previous approaches to fibre-based optically synchronized systems are less than optimal; super-continuum generation^{20–22} does not scale to sufficiently high power, implementation of a fibre-based OPO has proven challenging²⁴ and unseeded four-wave mixing requires low repetition rates²³, which ultimately limit the imaging speed. Here, we combine the advantages of optical synchronization with straightforward power scaling in fibre amplifiers.

A remaining challenge for amplified fibre lasers compared to high-power free-space lasers is the presence of high-frequency laser noise^{22,26}. We present the implementation of a noise suppression scheme based on autobalanced detection^{27,28}. Compared to previous implementations that suffer from low speed²¹ or a limited noise cancellation bandwidth²⁶, we have developed detection electronics optimized for high-speed microscopy. We present sensitive SRS imaging with uncompromised performance with our novel fibre laser source.

Results

The laser system is based on the key realization that the difference frequency of the two major fibre gain media, erbium and ytterbium, corresponds to the high-wavenumber region of Raman spectra²⁵, where most SRS imaging is performed. We have implemented an all-fibre dual-wavelength laser system based on optical synchronization of two picosecond amplifiers using a broadband super-continuum and have optimized the pulse parameters for high-speed SRS imaging.

Figure 1b presents a detailed schematic of our tunable dual-wavelength fibre laser source. It starts with an Er-doped fibre oscillator at 1,560 nm that is mode locked with a carbon nanotube (CNT)

¹Invenio Imaging, Inc., 1600 Adams Dr, Menlo Park, California 94025, USA, ²Department of Chemistry and Chemical Biology, Harvard University, 12 Oxford Street, Cambridge, Massachusetts 02138, USA, ³College of Optical Science, University of Arizona, 1630 E University Boulevard, Tucson, Arizona 85721, USA; [†]These authors contributed equally to this work. *e-mail: xie@chemistry.harvard.edu; kkieu@optics.arizona.edu

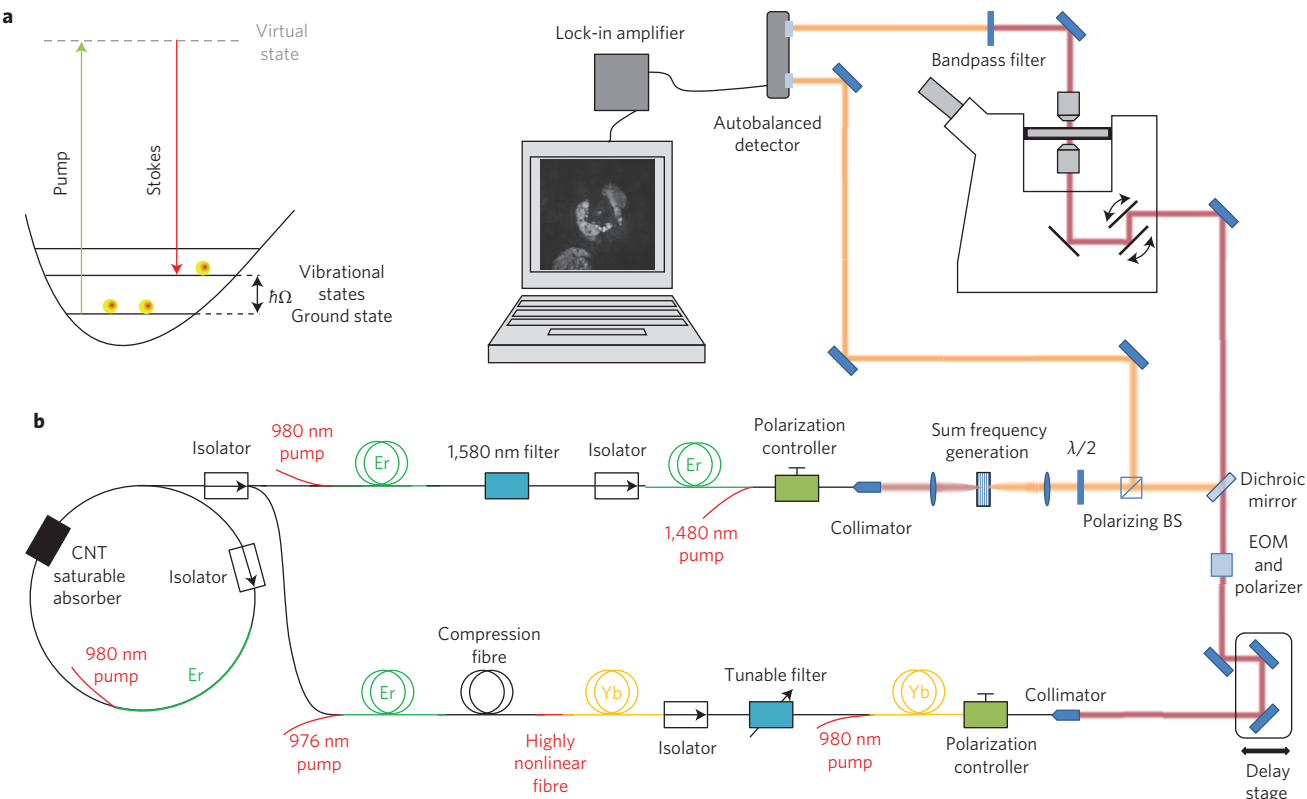


Figure 1 | Schematic of the fibre-laser system and SRS microscope. **a**, Energy diagram for SRS. When the difference in photon energy between the pump and Stokes beams matches the energy of a vibrational state of the target molecule, $\hbar\Omega$, molecules are efficiently excited from the ground state to the corresponding excited state and a pump photon is absorbed (stimulated Raman loss, SRL) and a Stokes photon is generated (stimulated Raman gain, SRG). **b**, Schematic of the fibre laser. The laser system starts with an Er-doped fibre oscillator, which is mode-locked with a carbon nanotube (CNT) saturable absorber. The output is split into two arms to generate the pump (upper arm) and Stokes (lower arm) beams. The Stokes beam is modulated at 10 MHz with an electro-optic modulator (EOM), temporally and spatially combined with the pump beam, and aligned into a beam-scanning microscope. Transmitted beams are collected with a condenser. The pump beam is detected by the autobalanced detector after the Stokes beam is blocked with an optical filter. The reference beam is sampled in front of the microscope with a polarizing beamsplitter (BS).

saturable absorber²⁹ at a repetition rate of 59 MHz. The output power of the oscillator is 7 mW and is split into two arms to generate the pump and Stokes beams for SRS.

The first arm is amplified to 80 mW in a normal-dispersion Er-doped preamplifier. Its output is broadened due to self-phase modulation (SPM) and we use a narrowband filter to reduce the bandwidth for SRS. The power (~2.2 mW after filtering) is restored in a low-nonlinearity Er-doped power amplifier. Its output could directly provide the Stokes beam for SRS. However, most multi-photon microscopes are optimized for transmission in the wavelength range 400–1,100 nm and we frequency double the output in a periodically poled lithium niobate (PPLN) crystal (Covesion, MSHG1550-1.0-10). With a conversion efficiency of ~45%, we obtain a near-infrared pump beam for SRS with up to 75 mW average power.

The second arm is frequency shifted in a super-continuum generator unit based on a highly nonlinear fibre (HNLF). Stable super-continuum generation requires the use of a short piece of HNLF. By careful optimization of the splice between the single-mode fibre and the HNLF, it is possible to reduce the splice loss to <1 dB, enabling all-fibre implementation. The output covers a range from 950 nm to >1,700 nm (the detection limit of the optical spectrum analyser)³⁰. We then use an Yb-doped preamplifier to increase the power of the spectral range around 1 μm to 40 mW (refs 30,31) and a narrowband filter to produce a picosecond pulse train that can be amplified in a low-nonlinearity Yb-doped power amplifier. We now have a narrowband Stokes beam with up to 120 mW average power that is synchronized to the oscillator and thus the pump beam.

Precise tuning of the difference frequency between pump and Stokes beams is achieved with motorized tunable filters. The outputs of the Er- and Yb-doped amplifiers are tunable from 1,530 nm to 1,590 nm (Fig. 2a) and from 1,010 nm to 1,060 nm (Fig. 2b), respectively. For fast tuning, we keep the pump beam fixed (the phase-matching wavelength of the PPLN crystal is temperature-controlled) and only tune the Stokes beam. Specifically, to access Raman spectra in the high-wavenumber region from 2,800 to 3,100 cm⁻¹, we frequency-double the fixed wavelength Er-arm at 1,580 nm to 790 nm (Fig. 2c) and tune the Yb-arm from 1,015 nm to 1,045 nm with <0.1 nm tuning accuracy (Agiltron, FOTF-01-6).

The pulse parameters were optimized specifically for SRS imaging of biological specimens by choosing the bandwidths of the narrowband filters and the length of the oscillator cavity. Our theoretical modelling (see Supplementary Section ‘Interpretation of the ANSI standard’) indicates that the signal-to-noise ratio (SNR) does not depend on the exact laser duty factor (Supplementary Fig. 1a) as nonlinear photodamage limits the maximum permissible peak power^{32–34}. However, at lower duty factors, higher average power is required to achieve the same SNR (Supplementary Fig. 1b). With the American National Standards Institute (ANSI) safety standard for clinical use in mind (see Supplementary Section ‘Interpretation of the ANSI standard’), it is thus advantageous to increase the duty factor compared to the solid-state OPO laser system, which has a pulse duration of 6 ps and repetition rate of 80 MHz.

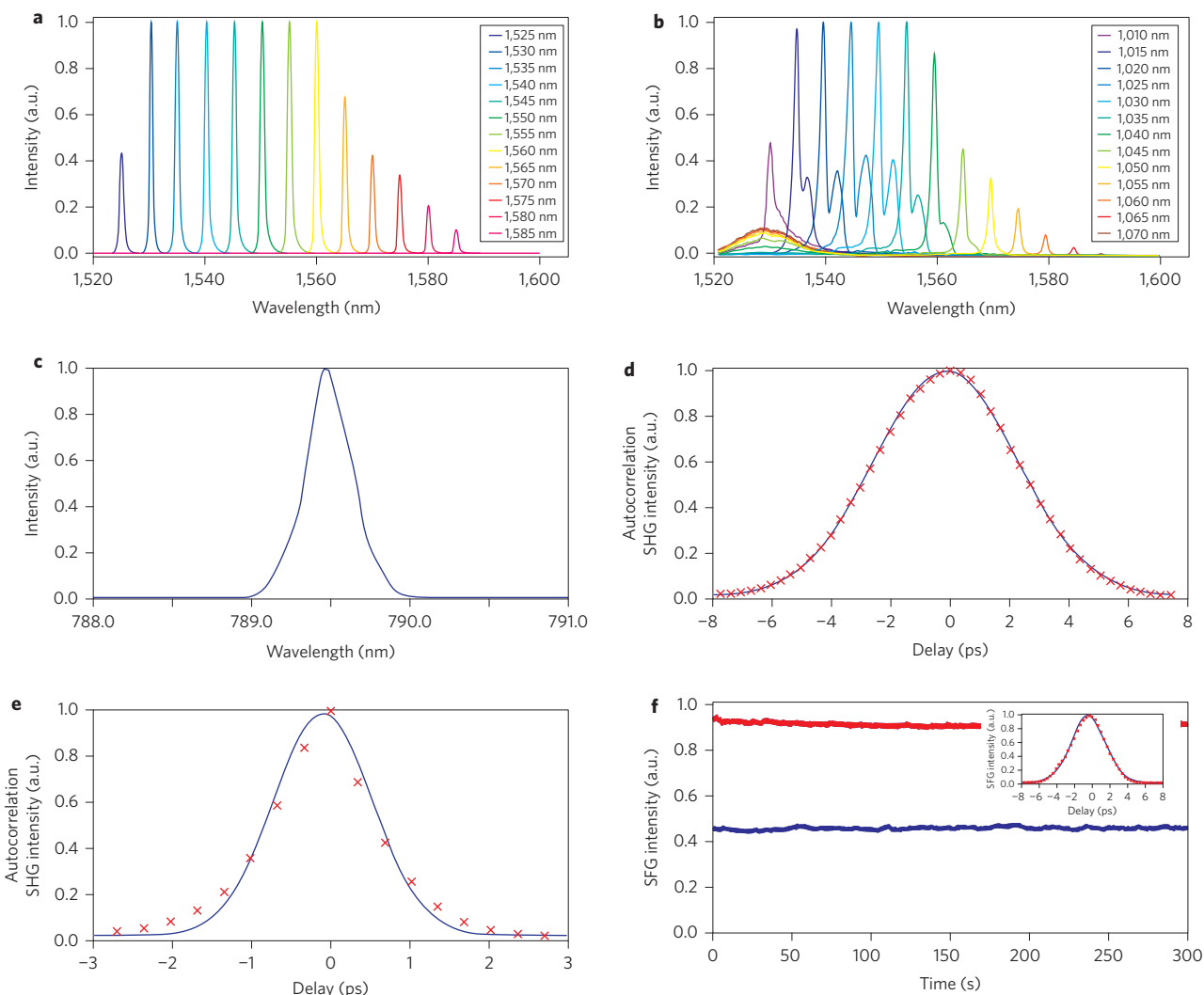


Figure 2 | Characterization of the fibre-laser source. **a,b,c,** Tuning ranges of the Er- and Yb-doped fibre power amplifiers, respectively. The Er-arm is frequency doubled to provide the pump beam. The Yb-arm provides the Stokes beam. **d,e,** Optical autocorrelations of the pump and Stokes pulses. **f,** Measurement of the timing jitter. Intensity noise at the peak (red) and half-maximum (blue) of the optical cross-correlation (inset) over 5 min.

We chose filters with a bandwidth of 1.2 nm (Fig. 2b), which approaches the required spectral resolution limit for SRS while still providing high peak power. Figure 2d shows the autocorrelation of the Stokes beam at 1,030 nm. The pulse duration of 1.0 ps was calculated by dividing the full-width at half-maximum (FWHM) by $\sqrt{2}$. This corresponds to a time-bandwidth product of a transform-limited pulse and, at 59 MHz repetition rate, provides a duty factor increase of about $\times 8$ compared to the solid-state OPO laser system. Figure 2e shows the autocorrelation of the pump beam with a pulse duration of 4.0 ps. The time-bandwidth product of 0.68 is about $\times 2$ larger than the transform limit, which is not fundamental. In a further optimized version of the laser source, we will aim to match the pulse duration of the pump and Stokes pulses.

The two beams are spatially overlapped with a free-space dichroic mirror. The rough time delay is adjusted by adding undoped fibre before the Yb-doped power amplifier. Fine delay is obtained by adjusting a mechanical delay line (Fig. 1b) while monitoring the sum-frequency generation (SFG) signal from a beta barium borate (BBO) crystal. This set-up was also used to measure the cross-correlation of the two pulse trains and determine the timing jitter. Figure 2f shows a 5 min time trace of the SFG signal at the half-maximum of the cross-correlation. Using the slope of the cross-correlation to convert from amplitude to timing fluctuations, the

timing jitter is estimated to be <24 fs. Such an approach only provides an upper limit estimate as laser intensity fluctuations can be falsely interpreted as timing jitter. However, it is sufficient to demonstrate that the timing jitter is much smaller than the cross-correlation bandwidth of 4.4 ps and does not affect the SRS imaging capabilities.

After careful optimization of the noise performance of the Er-arm, we obtained a pump beam that is ~ 27 dB above the shot-noise floor at 28 mW average power (Supplementary Fig. 3). Anything other than shot-noise-limited performance is not acceptable for SRS microscopy, as it limits the ability to detect low-concentration molecular species. The general idea of balanced detection (Fig. 3a) is that a portion of the pump beam can be sampled at the laser output (Fig. 1b). Laser noise other than the shot noise is common to both the sample and reference arms, and subtracting the two results in suppression of such common-mode noise. As the modulated signal only appears in the sample arm, it is not subtracted and can be detected with demodulation electronics (for example, a lock-in amplifier) with shot-noise-limited sensitivity (Fig. 3a).

In theory, balanced detection can reduce the laser noise to 3 dB above the shot noise, because it also introduces the shot noise of the reference arm. In practice, noise cancellation depends on the exact balance of the two arms. For example, if the intensity of the

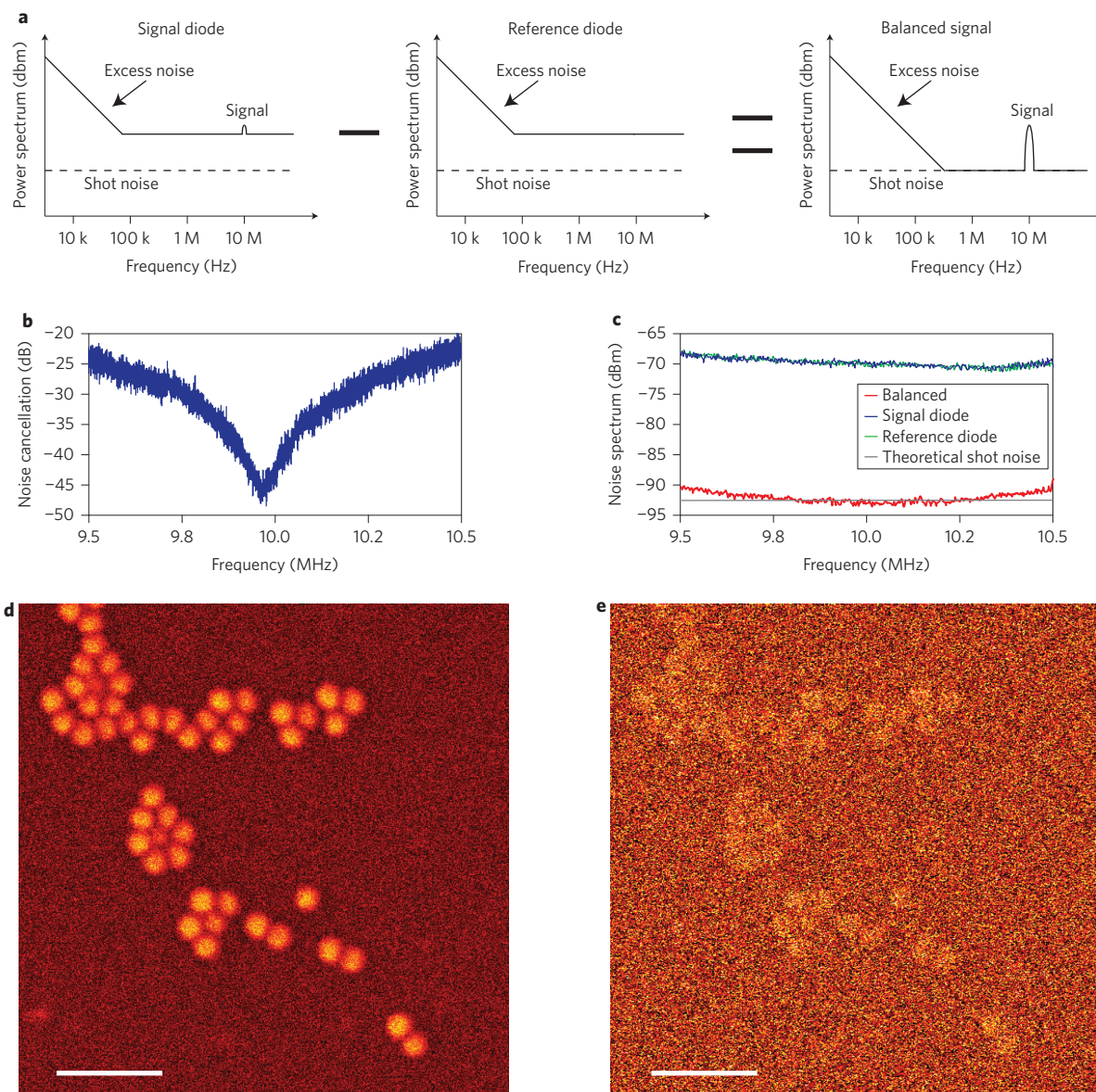


Figure 3 | Autobalanced detection. **a**, Principle of balanced detection. **b**, Noise suppression of the home-built autobalanced detector optimized for a 10 MHz signal. **c**, Noise spectrum of the fibre laser with (red) and without (blue) autobalanced detection. The theoretical shot noise is indicated in grey. **d,e**, SRS images of 1.1 μm polystyrene beads with (**d**) and without (**e**) autobalanced detection. Scale bars, 5 μm.

sample arm is only 90% of the reference arm, noise is suppressed by a factor of 10 or 20 dB. Application of the technique to microscopy would thus be limited by varying the sample transmission. To ensure maximum suppression independent of the sample transmission, we implement ‘auto’-balanced detection and rely on the d.c. signals from both arms to control the gain of the reference arm to balance the signals before subtraction. This approach takes advantage of the timescale separation of the modulation, the auto-balancing speed and the pixel dwell time. However, commercially available balanced detectors do not meet these timing requirements and their use drastically reduces the imaging speed²².

To overcome this limitation, we have developed a voltage-subtraction autobalanced detector for the specific requirements of high-speed microscopy. A detailed schematic is shown in Supplementary Fig. 2. Identical large-area silicon diodes are used for the sample and reference arms to accommodate the optical power. The a.c. and d.c. signals of each arm are then separated. The a.c. signals are filtered around the modulation frequency (10 MHz) and preamplified by trans-impedance amplifiers to overcome electronic noise.

A four-channel variable-gain amplifier (VGA) amplifies the filtered a.c. and d.c. signals of the two arms and a proportional integral derivative loop feedback circuit is used to control the gain of the reference arm to lock the d.c. levels. Because a.c. and d.c. signals experience the same gain in each channel, this generates the autobalancing of the a.c. signals before subtraction in a differential amplifier.

Our autobalanced detector allows a noise suppression of >40 dB at 10 MHz (Fig. 3b), which is significantly more than the laser excess noise. We thus achieve shot-noise-limited detection sensitivity (Fig. 3c). The noise suppression bandwidth of our implementation is currently limited by the dispersion of the specific phase shifters, which is not fundamental and is sufficiently large (500 kHz) to allow removal of all excess noise at the sampling speeds required for 1 frame s⁻¹ imaging. The 3 dB point of the autobalancing loop (data not shown) is chosen at ~500 kHz to compensate for pixel-to-pixel transmission variation.

For SRS imaging, the Stokes beam is modulated at 10 MHz with an electro-optic modulator (Thorlabs, EO-AM-NR-C2) and combined with the pump beam using a dichroic mirror. The collinear

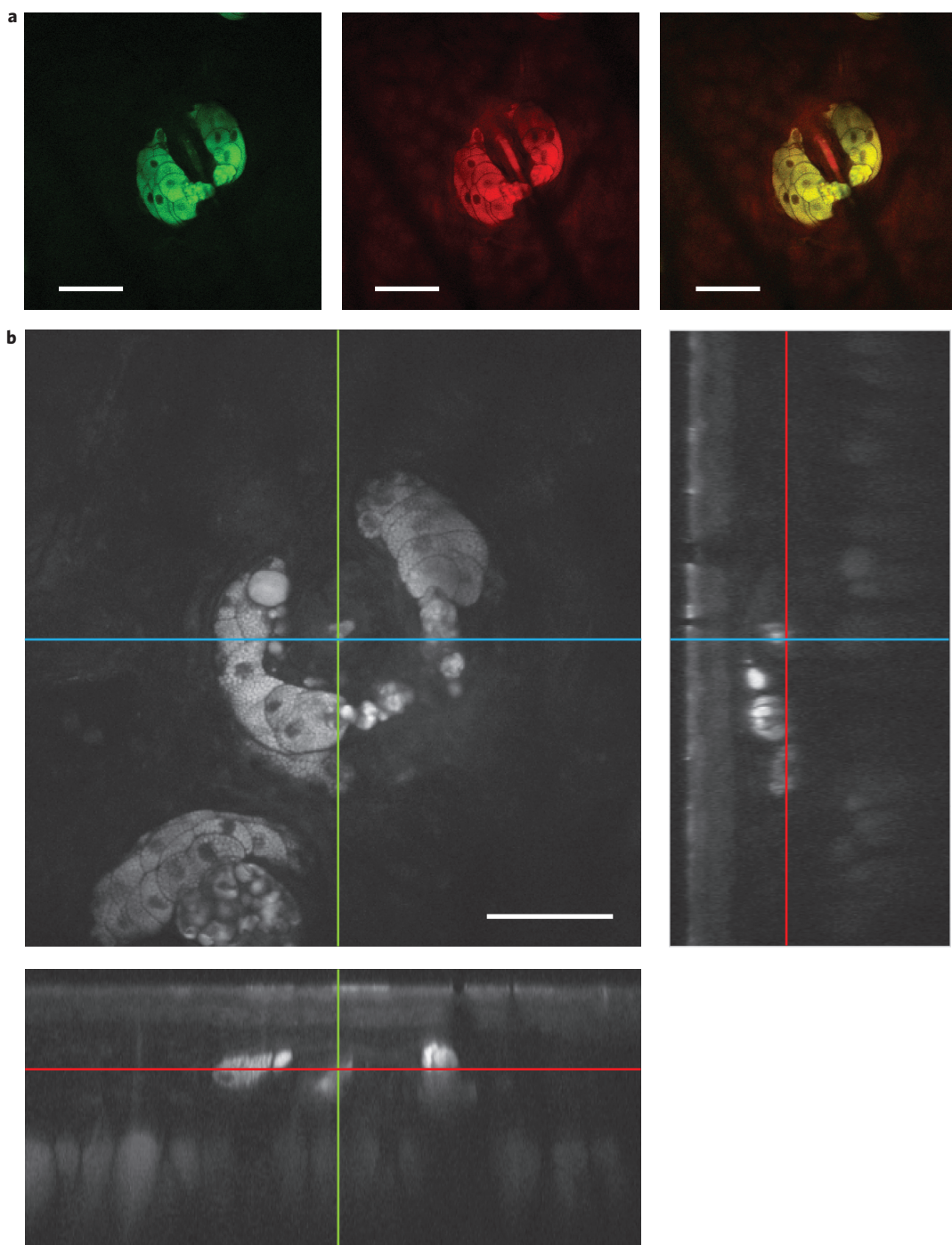


Figure 4 | SRS spectral imaging with the fibre-laser source. **a**, Two-colour image of a sebaceous gland in mouse skin acquired at 2,850 cm⁻¹ (mainly lipids, green), at 2,950 cm⁻¹ (mainly proteins, red) and the composite of the two colours. **b**, z-stack acquired at 1 frame s⁻¹ and cross-sections from different directions. Scale bars, 50 μ m.

beams are directed into a beam-scanning microscope (Olympus, IX71) and focused into the sample with a water immersion objective (Olympus, UPLANSAPO 60XW, 1.2 NA). The transmitted beams are collected with an oil immersion condenser (Nikon, 1.4 NA), the Stokes beam is blocked with a high-optical-density filter (Chroma, CARS890/220), and the pump beam is detected with the signal arm of the autobalanced detector. The reference beam is generated with a polarization beamsplitter and the rough balance is set with a half-wave plate before imaging. The output of the autobalanced detector is then sent to a custom lock-in amplifier⁹ to detect the 10 MHz SRS signal.

Figure 3d,e presents SRS images of 1.1 μ m polystyrene beads acquired at an imaging speed of 1 frame s⁻¹ and with 24 mW power at the focus with (Fig. 3d) and without (Fig. 3e) autobalancing. Balanced detection improves the SNR by a factor of 10.6, from 0.5 to 5.3. No image artefact due to varying sample transmission is visible, even at the edges of the beads (Supplementary Fig. 4).

Figure 4a shows multicolour SRS imaging of mouse skin samples. The green channel in Fig. 4a was acquired at the CH₂-stretching vibration of lipids (2,850 cm⁻¹) and the red channel at the CH₃-stretching vibration of proteins (2,950 cm⁻¹). The images show a lipid-rich sebaceous gland wrapped around a protein-rich hair.

Figure 4b shows a 100- μm -deep stack acquired every 1 μm at a frame rate of 1 frame s^{-1} (Supplementary Movie 1 shows the complete z-stack). This is the fastest SRS imaging experiment performed with a fibre laser source to date, reaching a performance equivalent to that of the more expensive state-of-the-art solid-state laser systems.

To demonstrate the ‘robustness’ of the laser system we performed imaging on a table that was not vibration isolated and in an environment that was not climate controlled (Supplementary Fig. 5). We also demonstrated the performance of the laser in response to external shock (Supplementary Movie 2) and ultra-long-term imaging over 44 h without adjusting the laser (Supplementary Movie 3).

Discussion

We have developed a dual-wavelength fibre laser source for SRS microscopy that is precisely tunable over the entire high-wavenumber region of Raman spectra, where most SRS imaging is performed. To reach the performance of solid-state laser systems we optimized the laser amplifiers and developed a broadband voltage-subtraction autobalanced detector. We demonstrate SRS imaging at an imaging speed up to 1 frame s^{-1} with shot-noise-limited sensitivity. The major advantages of our fibre-laser SRS system are (1) operation that does not require a vibration-isolated optical table, (2) operation in environments that are not climate controlled and (3) reduced cost. It has the promise to extend the use of SRS microscopy to non-expert users and facilitate clinical applications. Towards this goal, demonstrating high-quality imaging at excitation powers that are compliant with the ANSI safety standard is a major milestone.

The major limitation of the current proof-of-concept implementation is the use of non-polarization-maintaining (PM) components and the fact that adjustment of the polarization state of the output is required to maintain the maximum SRS signal. All components are available as PM versions, and an all-PM design is conceivable based on the same set-up. The use of large-mode-area components will further reduce SPM broadening and increase spectral fidelity. Care will need to be taken to achieve better matching of the pump and Stokes beam pulse durations. All-fibre delivery is further required to fully take advantage of the properties of fibre lasers. Finally, system integration of the microscope and fibre laser will enable automated spectral SRS imaging, and the development of an integrated hand-held SRS scanner is under way.

Methods

Laser spectra were measured with an optical spectrum analyser (HP, 70951A) with a spectral resolution of 0.1 nm. Optical autocorrelations were performed with a home-built background-free autocorrelator based on a 1 mm BBO crystal (Witcore, BBO 6-6-1 mm) and a manual delay stage. The timing jitter measurements were acquired with the same set-up. Relative intensity noise spectra were acquired with a radiofrequency spectrum analyser (Sigmalhounds, USB-SA44B) following ref. 35. The bandwidth of the spectrum analyser for the measurements in Fig. 3b,c was 400 Hz. We used a large-area silicon photodiode (OSI Optoelectronics, S-100CL) back-biased at 48 V to provide both dynamic range as well as response time. The d.c. signal was separated with a bias-T (Minicircuits, ZFBT-4R2GW+) and recorded with an oscilloscope to provide the intensity calibration of the relative intensity noise measurement (Supplementary Fig. 3). The shot-noise level was estimated following ref. 35, given the measured d.c. signal. The suppression ratio of the balanced detector was measured with the radiofrequency spectrum analyser by artificially increasing the noise of the fibre laser with an acousto-optic modulator driven by a white-noise signal from a radiofrequency function generator.

Received 8 July 2013; accepted 6 December 2013;
published online 19 January 2014

References

- Zumbusch, A., Holtom, G. R. & Xie, X. S. Three-dimensional vibrational imaging by coherent anti-Stokes Raman scattering. *Phys. Rev. Lett.* **82**, 4142–4145 (1999).
- Evans, C. L. & Xie, X. S. Coherent anti-Stokes Raman scattering microscopy: chemical imaging for biology and medicine. *Annu. Rev. Anal. Chem.* **1**, 883–909 (2008).
- Ploetz, E., Laimgruber, S., Berner, S., Zinth, W. & Gilch, P. Femtosecond stimulated Raman microscopy. *Appl. Phys. B* **87**, 389–393 (2007).
- Freudiger, C. W. *et al.* Label-free biomedical imaging with high sensitivity by stimulated Raman scattering microscopy. *Science* **322**, 1857–1861 (2008).
- Ozeki, Y., Dake, F., Kajiyama, S., Fukui, K. & Itoh, K. Analysis and experimental assessment of the sensitivity of stimulated Raman scattering microscopy. *Opt. Express* **17**, 3651–3658 (2009).
- Nandakumar, P., Kovalev, A. & Volkmer, A. Vibrational imaging based on stimulated Raman scattering microscopy. *New J. Phys.* **11**, 033026 (2009).
- Bloembergen, N. The stimulated Raman effect. *Am. J. Phys.* **35**, 989–1023 (1967).
- Evans, C. L. *et al.* Chemical imaging of tissue *in vivo* with video-rate coherent anti-Stokes Raman scattering microscopy. *Proc. Natl Acad. Sci. USA* **102**, 16807–16812 (2005).
- Saar, B. G. *et al.* Video-rate molecular imaging *in vivo* with stimulated Raman scattering. *Science* **330**, 1368–1370 (2010).
- Ganikhhanov, F., Evans, C. L., Saar, B. G. & Xie, X. S. High-sensitivity vibrational imaging with frequency modulation coherent anti-Stokes Raman scattering (FM CARS) microscopy. *Opt. Lett.* **31**, 1872–1874 (2006).
- Min, W., Freudiger, C. W., Lu, S. & Xie, X. S. Coherent nonlinear optical imaging: beyond fluorescence microscopy. *Annu. Rev. Phys. Chem.* **62**, 507–530 (2011).
- Owyong, A. Sensitivity limitations for CW stimulated Raman spectroscopy. *Opt. Commun.* **22**, 323–328 (1977).
- Ozeki, Y. *et al.* Stimulated Raman scattering microscope with shot noise limited sensitivity using subharmonically synchronized laser pulses. *Opt. Express* **18**, 13708–13719 (2010).
- Ji, M. *et al.* Rapid, label-free detection of brain tumors with stimulated Raman scattering microscopy. *Sci. Transl. Med.* **5**, 201ra119 (2013).
- Lin, C.-Y. *et al.* Picosecond spectral coherent anti-Stokes Raman scattering imaging with principal component analysis of meibomian glands. *J. Biomed. Opt.* **16**, 021104 (2011).
- Ozeki, Y. *et al.* High-speed molecular spectral imaging of tissue with stimulated Raman scattering. *Nature Photon.* **6**, 845–851 (2012).
- Kong, L. *et al.* Multicolor stimulated Raman scattering microscopy with a rapidly tunable optical parametric oscillator. *Opt. Lett.* **38**, 145–147 (2013).
- Ganikhhanov, F. *et al.* Broadly tunable dual-wavelength light source for coherent anti-Stokes Raman scattering microscopy. *Opt. Lett.* **31**, 1292–1294 (2006).
- Jones, D. J. *et al.* Synchronization of two passively mode-locked, picosecond lasers within 20 fs for coherent anti-Stokes Raman scattering microscopy. *Rev. Sci. Instrum.* **73**, 2843–2848 (2002).
- Pegoraro, A. F. *et al.* Optimally chirped multimodal CARS microscopy based on a single Ti:sapphire oscillator. *Opt. Express* **17**, 2984–2996 (2009).
- Krauss, G. *et al.* Compact coherent anti-Stokes Raman scattering microscope based on a picosecond two-color Er:fiber laser system. *Opt. Lett.* **34**, 2847–2849 (2009).
- Gambetta, A. *et al.* Fiber-format stimulated-Raman-scattering microscopy from a single laser oscillator. *Opt. Lett.* **35**, 226–228 (2010).
- Baumgartl, M. *et al.* All-fiber laser source for CARS microscopy based on fiber optical parametric frequency conversion. *Opt. Express* **20**, 4484–4493 (2012).
- Lefrancois, S. *et al.* Fiber four-wave mixing source for coherent anti-Stokes Raman scattering microscopy. *Opt. Lett.* **37**, 1652–1654 (2012).
- Bégin, S. *et al.* Coherent anti-Stokes Raman scattering hyperspectral tissue imaging with a wavelength-swept system. *Biomed. Opt. Express* **2**, 1296–1306 (2011).
- Noze, K. *et al.* Sensitivity enhancement of fiber-laser-based stimulated Raman scattering microscopy by collinear balanced detection technique. *Opt. Express* **20**, 13958–13965 (2012).
- Hobbs, P. C. D. Shot noise limited optical measurements at baseband with noisy lasers. *Proc. SPIE* **1376**, 216–221 (1991).
- Hobbs, P. C. D. *Building Electro-optical Systems: Making It All Work* (Wiley, 2000).
- Kieu, K. & Mansuripur, M. Femtosecond laser pulse generation with a fiber taper embedded in carbon nanotube/polymer composite. *Opt. Lett.* **32**, 2242–2244 (2007).
- Kieu, K., Jones, J. & Peyghambarian, N. High power femtosecond source near 1 micron based on an all-fiber Er-doped mode-locked laser. *Opt. Express* **18**, 21350–21355 (2010).
- Andrianov, A., Anashkina, E., Muravyev, S. & Kim, A. All-fiber design of hybrid Er-doped laser/Yb-doped amplifier system for high-power ultrashort pulse generation. *Opt. Lett.* **35**, 3805–3807 (2010).
- Hopt, A. & Neher, E. Highly nonlinear photodamage in two-photon fluorescence microscopy. *Biophys. J.* **80**, 2029–2036 (2001).
- Fu, Y., Wang, H., Shi, R. & Cheng, J.-X. Characterization of photodamage in coherent anti-Stokes Raman scattering microscopy. *Opt. Express* **14**, 3942–3951 (2006).
- Nan, X., Potma, E. O. & Xie, X. S. Nonperturbative chemical imaging of organelle transport in living cells with coherent anti-Stokes Raman scattering microscopy. *Biophys. J.* **91**, 728–735 (2006).

35. Obarski, G. E. & Hale, P. D. How to measure relative intensity noise in lasers. *Laser Focus World* **35**, 273–278 (1999).

Acknowledgements

The authors thank P. Hobbs, J. McArthur and J. Trautman for discussions. The authors thank D. Fu and F.-K. Lu for help with sample preparation. This material is based on work supported by the National Science Foundation (NSF; grant no. 1214848 to C.W.F.) and by the National Institutes of Health (NIH; grant no. 5R01EB010244 to X.S.X.). This work was performed in part at the Center for Nanoscale Systems (CNS), a member of the National Nanotechnology Infrastructure Network (NNIN), which is supported by the NSF (under grant no. ECS-0335765). CNS is part of Harvard University. KK and NP would like to acknowledge the support from the CIAN NSF ERC under grant #EEC-0812072 and the State of Arizona's TRIF funding.

Author contributions

C.W.F. and K.Q.K. designed and characterized the fibre-laser system. W.Y. and G.R.H. designed and characterized the autobalanced detector. C.W.F. and W.Y. performed the

imaging experiments. C.W.F., X.S.X., N.P. and K.Q.K. conceived the project and supervised its implementation. C.W.F., W.Y., K.Q.K., N.P. and X.S.X. wrote the manuscript and all authors commented on it.

Additional information

Supplementary information is available in the online version of the paper. Reprints and permissions information is available online at www.nature.com/reprints. Correspondence and requests for materials should be addressed to X.S.X. and K.Q.K.

Competing financial interests

Harvard University and University of Arizona has filed a patent application based on the current work. C.W.F. and X.S.X. have financial interests in Invenio Imaging Inc. K.Q.K. has financial interests in KPhotonics LLC. Any opinions, findings, conclusions or recommendations expressed in this material are those of the authors and do not necessarily reflect the views of the NSF or NIH.